JOURNAL OF MATERIALS SCIENCE 33 (1998) 2235–2249

Review
Metal nanoclusters in glasses as non-linear photonic materials

P. CHAKRABORTY
Saha Institute of Nuclear Physics, 1/AF Bidhannagar, Calcutta 700 064, India
E-mail: pchakra@hpz.saha.ernet.in

Although electronics technologies have made great advances in device speed, optical devices can function in the time domain inaccessible to electronics. In the time domain less than 1 ps, optical devices have no competition. Photonic or optical devices are designed to switch and process light signals without converting them to electronic form. The major advantages that these devices offer are speed and preservation of bandwidth. The switching is accomplished through changes in refractive index of the material that are proportional to the light intensity. The third-order optical susceptibility, $\chi^{(3)}$, known as the optical Kerr susceptibility which is related to the non-linear portion of the total refractive index, is the non-linearity which provides this particular feature. Future opportunities in photonic switching and information processing will depend critically on the development of improved photonic materials with enhanced Kerr susceptibilities, as these materials are still in a relatively early stage of development. Optically isotropic materials, e.g. glasses that have inversion symmetry, inherently possess some third-order optical non-linearities. Although this is quite small for silica-glasses at $\lambda = 1.06\ \mu m$, the absorption coefficient is extremely low, thereby allowing all-optical switching between two waveguides, embedded in a silica fibre, simply by controlling the optical pulse intensity. Different glass systems are now under investigation to increase their non-linearity by introducing a variety of modifiers into the glass-network. The incorporation of semiconductor microcrystallites enhances the third-order optical response. Metal colloids or nanoclusters, embedded in glasses, have also been found to introduce desired third-order optical non-linearities in the composite at wavelengths very close to that of the characteristic surface-plasmon resonance of the metal clusters. Ion implantation is nowadays an attractive method for inducing colloid formation at a high local concentration unattainable by the melt-glass fabrication process and for confining the non-linearities to specific patterned regions in a variety of host matrices. Recent works on metal-ion implanted colloid generation in bulk silica glasses have shown that these nanocluster–glass composites under favourable circumstances have significant enhancement of $\chi^{(3)}$ with picosecond temporal responses. The remarkable achievements in developing such novel photonic materials seem to open the way for advances in all-optical switching devices, e.g. in inducing metal-colloids into coupled waveguides acting as a directional coupler. The present paper addresses the phenomena of optical non-linearities in metal nanocluster–glass composites that are synthesized by ion implantation, and the potential uses of these novel composite materials in photonics.

1. Introduction

Before the advent of lasers, transparent optical materials were assumed to be essentially passive, unaffected by light travelling through them. The high powers of laser beams made it possible, for the first time, to observe that the effect of light on a medium can indeed change its properties, e.g. refractive index or absorption. These are optical non-linear phenomena. When this happens, the light itself also gets affected by this change in a non-linear way; for example, the non-linear response of the material can convert the laser light into new colours, both harmonics of the optical frequency and sum and difference frequencies.

A currently active area of non-linear optics research is concerned with all-optical devices that are designed to switch and process light signals without converting them to electronic form, thus eliminating the electronic "bottleneck" in the speed of electronics used for switching, routing and signal processing. These devices are essentially based on the non-linear optical

properties of materials, i.e. changes of the refractive index caused by an intense optical beam or by an applied electric field. Conceptually, the simplest type of a photonic switch is a directional coupler in which the optical coupling from one waveguide to the other is achieved by only changing the intensity of the input optical beam. The most mature technology for directional coupler switches is based on the well-known linear electro-optic (LEO) effect in $LiNbO_3$ waveguides. In this, an applied voltage changes the refractive index of the material, thereby altering the optical phase of the signals propagating within. In a $LiNbO_3$ 2×2 cross point (two inputs, two outputs) the coupler length is typically 1 cm and the drive voltage is about 10 V. Such devices are capable of providing extremely high switching speeds and can increase the aggregate transmission bandwidth. If the change in refractive index, Δn, per applied electric field, E, is small, a long device-length is needed to accumulate the necessary optical phase shift, π, in the waveguide. Comparing the relative strengths of selected electro-refractive effects for various materials at optical fibre-communication wavelengths (1.3–1.55 μm) along with typical switching voltage–waveguide length products, it has been found that semiconductor waveguide structures like $Al_{0.25}Ga_{0.75}As/Al_{0.2}Ga_{0.8}As/Al_{0.25}Ga_{0.75}As$ with a large optical non-linearity at 1.55 μm, provide even more compact switches with lower switching energies and speeds comparable to the established $LiNbO_3$ electro-optic switches.

The effects have been found to be more pronounced in band-gap engineered materials. As the dimensions become reduced, from three-dimensional bulk semiconductors to two-dimensional quantum-well structures (and further to one-dimensional quantum-wires or to zero-dimensional quantum-dots), the ratio of index change to applied field in the active volume is increased. However, the real difficulty with electronics is that because electrons (fermions) are highly interactive, there occurs an inter-capacitance or stray capacitance amongst the electrons in the electronic signal before it reaches the gate of a transistor, thereby limiting the speed and consequently the bandwidth, and in effect, switching times of around < 500 ps can be considered to be high speed. Optical devices can, however, function in the time-domain inaccessible to electronics. In the time-domain below picosecond (say, femtoseconds), optical devices have no competition.

The advancements in photonic switching and information processing will depend critically on the developments of improved photonic materials, which are still in a relatively early stage of development. There is presently an intense interest in the possibility of developing a computer, based on all-optical switches. Such a switch could be feasible and competitive if switching times of less than 100 ps could be demonstrated at an energy consumption less than 1 pJ [1]. The suggestion was made [2] that the inherent small optical non-linearities of glasses could be utilized for switches of this type. It has been observed that semiconductor (e.g. PbS, CdS_xSe_{1-x}, etc.) microcrystallites or metal colloidal particles of dimensions typically in the range 1–20 nm, incorporated in transparent glassy materials, enhance the third-order optical non-linearity of the host matrices significantly.

The enhanced magnitudes of the optical non-linearities of such nanocluster–glass composites and the amazingly short temporal responses (in the time domain below picosecond) of these non-linearities, have unambiguously opened a new dimension in the arena of photonics, bringing the scientific community closer towards success in the realization of all-optical switching devices [3].

2. Non-linear optical (NLO) phenomena and their physical origins

Non-linear optics is traditionally introduced by noting that the dielectric susceptibility can be expanded in a Taylor series in terms of the oscillating optical electric field. In an isotropic medium the general relation between the polarization, P (dipole moment per unit volume), induced by the applied electric field E, is expressible as a Taylor expansion involving only the magnitude, because the direction of polarization coincides with that of the field, namely

$$P = \varepsilon(\chi^{(1)}E + \chi^{(2)}E + \chi^{(3)}E^3 + \dots) \qquad (1)$$

where ε is the dielectric constant of the medium. In this expansion, $\chi^{(1)}$ is the normal or linear dielectric susceptibility of the medium and contributes to all the phenomena associated with linear optics, such as reflection, refraction, interference, etc. It is generally much larger than the non-linear coefficients $\chi^{(2)}$, $\chi^{(3)}$ and so forth.

If the applied field has the form $E_0e^{-i\omega t}$, the induced polarization is

$$P = \varepsilon(\chi^{(1)}E_0e^{-i\omega t}\chi^{(2)}E_0^2e^{-i2\omega t} + \chi^{(3)}E_0^3e^{-i3\omega t} + \dots) \qquad (2)$$

That part of the polarization associated with second- and higher-terms gives rise to the generation of optical harmonics. These usually decrease rapidly in intensity with increasing order. If the general relation between P and E is such that a reversal of the direction of E merely results in the reversal of the direction of P, that is, if $P(E)$ is an odd function, then the even terms are all zero and there are no even harmonics. This is, in fact, the case with isotropic media, e.g. glasses.

In the case of crystalline media, P and E are not necessarily parallel. The polarization must then be expressed as an expansion of the type

$$P = \varepsilon(\chi^{(1)}E + \chi^{(2)}EE + \chi^{(3)}EEE + \dots) \qquad (3)$$

where $\chi^{(1)}$ is the ordinary susceptibility tensor. The coefficients $\chi^{(2)}$, $\chi^{(3)}$, and so forth, are higher-order tensors. The non-linear part of the total polarization can be written as

$$P^{\mathrm{NL}} = \varepsilon(\chi^{(2)}EE + \chi^{(3)}EEE + \dots) \qquad (4)$$

If the impressed field, E, is a light wave of angular frequency ω, then the second-harmonic polarization,

$P(2\omega)$, arises from the term $\varepsilon\chi^{(2)}EE$. Its components can be written as

$$P_i(2\omega) = \sum_j \sum_k \chi^{(2)}_{ijk} E_j E_k \tag{5}$$

The amount of second-harmonic light that is produced depends critically on the form of the $\chi^{(2)}$ tensor. In order for the $\chi^{(2)}$ tensor not to vanish, the crystal must not have any centre of symmetry. This is also one of the requirements for a crystal to be piezoelectric, such as quartz, potassium dihydrogen phosphate (KDP), etc.

The origin of the non-linear susceptibility can be viewed classically as the response of an electron driven by an electromagnetic field in an anharmonic potential well, resulting from the interatomic electric field, E, in the crystalline solid. When a light wave propagates through an optical medium, the oscillating electromagnetic field exerts a polarizing force on all of the electrons comprising the medium. Because the inner electrons of the atoms are tightly bound to the nuclei, the major polarizing effect is exerted on the outer or valence electrons. The intra-atomic field is of the order of $10\,\mathrm{V\,nm^{-1}}$ or $\sim 10^{10}\,\mathrm{V\,m^{-1}}$. For driving optical fields, E, much weaker than that, the polarization response is essentially linear. This produces a polarization which is proportional to the electric field of the light wave. For an intense optical field (i.e. comparable to or greater than the intra-atomic field) enough to drive the electron beyond the quadratic minimum of the interatomic potential, the response becomes increasingly non-linear. Based on the classical atomic model of non-linearity [4] (considering the motion of a one-dimensional anharmonic electron oscillator with damping, driven by a laser field), the ratio between the magnitudes of non-linear polarizations of successive orders can be expressed as

$$\left|\frac{P^{(n+1)}}{P^n}\right| \approx \frac{e|E|}{m\omega_0^2 r} \approx \frac{e|E|}{e|E_{\mathrm{at}}|} \tag{6}$$

where ω_0 is the oscillation frequency of the electron and r is the radius of the equilibrium orbital of the electron. ($m\omega_0^2 r$ is actually the expression for the linear force which is equal to $e|E_{\mathrm{at}}|$ where E_{at} is the intra-atomic electric field at a distance equal to the Bohr radius a_0.) Now $E_{\mathrm{at}} = e/a_0^2 = 5.15 \times 10^{11}\,\mathrm{V\,m^{-1}}$. Following the expression for energy flux density of an electromagnetic wave ($= \varepsilon c E^2$), the above value of E_{at} corresponds to a laser power of $7 \times 10^{20}\,\mathrm{W\,m^{-2}}$, where ε (dielectric constant of vacuum) $= 8.8 \times 10^{-12}$ and c (speed of light) $= 3 \times 10^8$, expressed in SI units.

At low light intensities, the optical fields are a small fraction of the molecules' total internal fields ($\sim 5 \times 10^{11}\,\mathrm{V\,m^{-1}}$). At high photon intensities, the induced fields become a significant fraction of the total. This added internal field substantially modifies the motions of the charges within the molecule and alters the nature of the polarization within the materials. Also, this added internal field "anharmonically" modifies the light wave's propagation, leading to remarkable effects when they occur coherently, constructively. That is when a material's properties (e.g. the interaction length for a process and the strength of the perturbation) are well-matched (i.e. phase-matched) to the laser wavelength, second- and third-order non-linear optical effects can drastically change the colour content or manner of propagation of light. Therefore, the non-linear phenomenon is evidenced by the changes in optical properties as the intensity of light is increased.

By 1965, all the basic non-linear optical frequency conversion phenomena – second harmonic generation (SHG), sum and difference frequencies and oscillation – had been demonstrated. Practical applications, however, were hampered by the limitations of available pump lasers and non-linear materials. The development of improved non-linear materials paralleled the evolution of improved pump lasers. A non-linear medium must meet several basic requirements. A reasonably large non-linear susceptibility is, of course, a prime consideration, but adequate birefringence for phase matching is equally important. Particularly attractive are the media that can be temperature-tuned to deliver non-critical phase matching at the desired wavelength. Because the second-order susceptibility must vanish in inversion symmetric media, almost all practical frequency-conversion is done with single crystals that lack inversion symmetry. Extensive materials research over the last decade has yielded several suitable second-order non-linear crystals, especially two ferroelectric niobates, $LiNbO_3$ and $Ba_2NaNb_5O_{15}$ which have non-linear susceptibilities an order of magnitude larger than KDP, or ammonium dihydrogen phosphate (ADP) crystals that were mostly used in early frequency conversion experiments. Later, materials like ternary semiconductors, such as $CdGeAs_2$ [5], $ZnGeP_2$ [6], Tl_3AsSe_3 [7], etc., alternative to the conventional SHG crystals (which absorb light in the mid-infrared region because of their oxygen content), were suggested to convert the frequency of the CO_2 laser operating at a wavelength of 10.5 μm, although these materials are not easy to produce and sometimes they show a low damage threshold. Recently, a new class of transparent materials for non-linear optical applications in the mid-infrared region has been reported [8]. These are ternary halides, such as $Tl_7Bi_3I_{16}$, Tl_3PbCl_5, etc., which have been found to be chemically stable and have properties like the absence of a centre of symmetry and the presence of birefringence, both necessary for an effective SHG. The importance of second harmonic generation lies in the fact that it is one of the principal methods of effective conversion of infrared radiation into visible and visible into ultraviolet. Third harmonic generation (THG) is possible in materials which are centrosymmetric, i.e. having inversion symmetry. The development of Q-switched lasers made it possible to generate third-harmonics in crystals [9], although the energy conversion efficiency in such cases was found to be quite low.

The physical origins of NLO phenomena can be categorized as either structural or compositional. Here "structural" refers to light-induced structure changes, such as a change of electronic density, average interatomic distances, molecular orientation,

phase transition, etc. These phenomena belong to the intrinsic category. The "compositional" refers to light-induced chemical composition changes which can be classified as the extrinsic type. This phenomenon consists essentially of light-induced chemical reactions (such as molecular dissociation, polymerization etc.). This can be either reversible or permanent.

Intrinsic non-linearity violates the principle of superposition arising from a non-linear response of the individual molecule unit-cell to the fields of two or more light waves, while extrinsic non-linearity is related to changes in the composition of the medium that result from the absorption or emission of light. In either type of non-linearity, the optical properties of the medium depend on the intensity of light and the order of non-linearity can be classified according to the power of the intensity involved. For example, in the case of harmonic generation (HG), the intensity of the nth harmonic is proportional to the nth power of the intensity of the fundamental, and in the optical Kerr effect the intensity of the Kerr signal is proportional to the product of probe-beam intensity and the square of the intensity of the pump-beam.

The optical Kerr effect can be defined as either light-induced double refraction or an intensity dependence of refractive index. The intensity-dependent refractive index, n, is usually expressed as

$$n = n_0 + n_2 I \tag{7a}$$

where n_0 is the linear refractive index of the material and is a function of $\chi^{(1)}$. Classical optics is concerned with this term in the low light intensity regime. I is the intensity of light averaged over a period and n_2 is the non-linear refractive index of the material. The total absorption, α, can similarly be expressed as

$$\alpha = \alpha_0 + \beta I \tag{7b}$$

where α_0 is the linear absorption coefficient and β is the coefficient characterizing the non-linear absorption and is known as the "two-photon absorption coefficient". Intensity-dependent refractive index (Equation 7a) and intensity-dependent absorption (Equation 7b) are both manifestations of non-resonant optical non-linearity. The non-resonant non-linearity is smaller than the resonant non-linearity but has a very fast response compared with the resonant non-linearity. The term "resonant non-linearities" refers to optical non-linearities at wavelengths close to linear absorption. In semiconductors, resonant optical non-linearities occur at wavelengths close to the bandgap absorption edge. Associated with resonant optical non-linearities are the transitions of electrons from the valence band to the conduction band. The electrons have a finite life time in the conduction band and then return to the valence band, leading to a finite recovery time for the non-linear optical effects. This time can be of the order of nanoseconds for a good quality semiconductor and is too slow in terms of switch speeds. On the other hand, "non-resonant non-linearities" refer to the optical non-linearities at photon energies below the band gap energy, E_g. It is possible for the light with photon energies in the range $E_g/2 < h\omega < E_g$ to be absorbed. A two-photon process is a process where two photons are involved (either emitted or absorbed) per real transition of an electron between the conduction and valence bands in the material. It can be regarded as a process where the electron, by absorbing one photon, makes a transition to a virtual intermediate state and makes a transition from the intermediate state to the final stable state by absorbing another photon. It must be emphasized that this transition cannot, in principle, be divided into a temporal sequence of events. It should be understood that both the photons are absorbed simultaneously, otherwise it would be equivalent to an absorption of two single photons. The two main requirements for the two-photon absorption are: (1) the energy for lifting the atom to the excited level should be double the energy of the exciting photon, and (2) the initial and final states should have the same parity. Two-photon absorption in an atomic system was first observed [10] on exciting caesium vapour with a ruby laser ($\sim 14\,400\,\mathrm{cm}^{-1}$). Emission of a fluorescence line at a wavelength of 584.7 nm, corresponding to the transition from $9D_{3/2}$ ($28\,828.9\,\mathrm{cm}^{-1}$) to $6P_{3/2}$ ($11\,735.49\,\mathrm{cm}^{-1}$) levels, indicated the occurrence of two-photon absorption.

For all-optical devices, the non-linear index of refraction and the two-photon absorption play critical roles; the latter, however, severely limits all-optical device performance [11]. The non-linear refractive index, n_2, and the two-photon absorption coefficient, β, are related to the real and imaginary parts of $\chi^{(3)}$, just as in linear optics the refractive index and absorption coefficient are related to the real and imaginary parts of linear susceptibility, $\chi^{(1)}$, respectively. In an amorphous material, e.g. glass, n_2 and β are related to the real and imaginary parts of $\chi^{(3)}$, i.e. $\mathrm{Re}[\chi^{(3)}]$ and $\mathrm{Im}[\chi^{(3)}]$, respectively by [12]

$$n_2 = \frac{12\pi}{n_0}\,\mathrm{Re}[\chi^{(3)}]$$

with

$$n_0 = (1 + 4\pi \mathrm{Re}[\chi^{(1)}])^{1/2} \tag{7c}$$

$$\beta = \frac{96\pi^2\omega}{n_0^2 c^2}\,\mathrm{Im}[\chi^{(3)}] \tag{7d}$$

where n_2 and $\chi^{(3)}$ are in e.s.u.

There are different ways to classify NLO materials. The criteria can be the order of non-linearity, the nature of the NLO interaction involved, or some characteristic of the material. Practically, the choice of a research subject in NLO materials is complicated by the fact that, for a given application, there are several potential candidates and each material has a few promising applications. In fact, there is a trade-off between non-linear response, optical loss, response time, laser power, device geometry, etc., disregarding other factors, such as chemical, thermal, and mechanical stabilities. Many simplifying, semi-empirical, self-consistent models have been proposed by researchers in high-power laser optics to predict the non-linear index coefficient of optical crystals and glasses [13]. It has been found that in the long-wavelength limit

(far removed from resonances) the non-linear index coefficient, n_2, scales with the linear refractive index [14]

$$n_2 = K\frac{n_d - 1}{\nu^{5/4}} \tag{7e}$$

where n_d is the linear refractive index of the material at the d-line of helium and ν is the Abbe number, which is the reciprocal of the wavelength dispersion of the linear refractive index of the material at this wavelength. Equation 7e involves a single constant $K(=391)$ for which the calculated values of $n_2(\sim 10^{-13}$ e.s.u) were found to be in reasonably good agreement with the experimental data over a wide range of optical materials [14]. This model assumes a single chemical component which determines linear and non-linear indices. For oxide glasses, this component is oxygen. The ability to predict n_2 empirically is quite good for low-index materials, but becomes more difficult when polarizable ions are present.

Much more extensive modelling of second-order non-linearities has been accomplished over the years. This non-linear process, i.e. second-harmonic generation, requires a crystal structure with lack of inversion symmetry, whereas the isotropic materials, such as glasses, have inversion symmetry and do not have any long-range periodicity unlike crystals. Therefore, the second-order contributions to the total polarization are usually ruled out in the case of glasses.

In most multicomponent oxide glasses, there are both bridging and non-bridging oxygens in the glass network (i.e. for a silicate glass, $Si–O^+Na^-$). These non-bridging ionic bonds possess larger n_2 than the bridging oxygen of the more covalent Si–O–Si bonds. A correlation between the non-bridging oxygen content and the non-linear indices was reported by Adair *et al.* [15]. In silicates modified with transition metal cations, optical properties are mostly determined by the concentration of metal cations rather than by the number of non-bridging oxygens, i.e. non-linearity is dominated by the bond-polarizability of the metal–oxygen bonds. Various kinds of glasses and their non-linearities, at wavelengths in the range 1.06–2 μm, were presented by Vogel *et al.* [16].

A distinction has to be considered as to whether the frequency of the applied optical field is resonant or non-resonant with an electronic transition in the material. In the non-resonant case, which is applicable to most of the glasses for wavelengths around 1 μm, the optical non-linearity is of electronic origin. The electronic non-linear response of glasses is generated by the electronic structure change due to the distortion of the electron orbits about the nuclei (polarizability) under the influence of a high intensity optical field. However, the non-linearities in glasses are small and require high optical intensities for switching. This drawback can, however, be compensated by the advantages due to an extremely low absorption coefficient and the high optical damage threshold of glasses for practical applications. As the origin of non-linearity is electronic and off-resonance, they have the fastest response times (of the order of femtoseconds), whereas, in the resonant case applicable to many semiconductors, GaAs/GaAlAs multiple quantum-wells, semiconductor-doped glasses, polymers, etc., the electronic structure change is due to the redistribution of electrons at different electronic states. In this case, non-linearities can be enhanced by several orders of magnitude but at the cost of higher power dissipation and slower responses. The response time in this case depends on the relaxation time of the carriers that are excited by the optical field.

3. Choice of non-linear materials

The choice of non-linear materials for practical applications is, however, not easy because there is no ideal material for all applications and as a result there is no universal definition of the figure of merit of materials for all applications. A good definition will ensure the proper selection of materials and is possible only after defining the application (e.g. generation of a frequency or all-optical switching), the characteristics of the device (e.g. dimension, geometry, acceptable loss, response time, and non-linear conversion efficiency), and the operation conditions (e.g. wavelength, power, and CW or pulse).

3.1. Non-linear materials for all-optical devices

NLO effects have important applications in optical communications where optical switching and optical signal processing devices are essential elements. The use of optics is advantageous over that of electronics because of the higher carrier frequency used, which gives a potentially higher bandwidth. The realization of optical circuit elements using NLO effects will overcome the limitations of the electronic modulation techniques to exploit the information carrying capacity of optical communication systems. The tremendous success in the development of high-silica glass fibres for light-wave transmission systems has stimulated investigations of new photonic devices. All-optical switching is based on either the spatial or temporal non-linear responses of materials. Various types of all-optical switching devices include non-linear directional couplers, non-linear mode sorters, non-linear distributed couplers, non-linear Mach–Zehnder interferometer, distributed feedback grating, etc. Each of the devices essentially uses some material with inherent $\chi^{(3)}$ or high-intensity optical field-induced $\chi^{(3)}$. A figure-of-merit is helpful in comparing materials for all optical devices but it must be formulated with a specific application in mind. A proposed figure-of-merit for non-linear materials compares the refractive index change created by the non-linear coefficient, n_2, with that caused by thermal effects [2]. The figure-of-merit is defined as

$$F = \frac{\text{fast index change required to produce switching}}{\text{resultant thermal index change}} \tag{8}$$

$$\approx \frac{\Delta n_{sat}}{\tau\alpha_0}$$

TABLE I Properties of non-linear optical materials

Material	$n_2(m^2\,W^{-1})$	$\alpha_0(cm^{-1})$	F
QW, GaAs/GaAlAs	10^{-8}	10^3	10^2
Polydiacetylenes	10^{-15}	10	10^4
Glass (Pb glass, Ti glass)	10^{-18}	10^{-2}	10^5

where τ is the response time or relaxation time of the non-linearity, n_{sat} is the change in refractive index at saturation and α_0 is the linear absorption coefficient. It is clear that an ideal non-linear material would have large non-linearity n_2, fast response time and minimal absorption in the wavelength range of interest. In addition, these materials must have thermal relaxation times which are sufficiently rapid so that there is no build-up of heat, because this would produce an effective refractive index just due to the change in temperature. This effective thermal non-linear index change can be expressed [17] as $[(dn/dT)(\alpha_0\tau_1/\rho C_p)](\tau/\tau_1)$ where dn/dT is the thermo-optic coefficient of the material, ρ is the density, C_p is the specific heat at constant pressure and τ_1 is the thermal relaxation time. The above expression can be approximated as $\tau\alpha_0$, as used in Equation 8.

The maximum operating speed of a device for serial pulses is determined by the non-linearity response time. Any non-linearity, even a thermal one, can be turned on instantaneously. However, in order to minimize cross-talk, it is important that the non-linear change in index induced by one pulse relaxes back to zero before the next pulse arrives. Therefore, the non-linearity relaxation time is a critical material parameter. Table I shows n_2, α_0 and F for several classes of materials [3]. Using this figure-of-merit, it is apparent that many glasses have larger F than other materials with much larger non-linear coefficients. The first ultrafast all-optical switch was demonstrated in silica glass fibre [18]. Although the non-linear index coefficient for silica at $\lambda = 1.06\,\mu m$ is small ($n_2 = 3.2 \times 10^{-20}\,m^2\,W^{-1}$), the absorption coefficient, α, is extremely small in silica fibres, thereby allowing all-optical switching between two waveguides embedded in the same optical fibre simply by controlling the optical pulse intensity.

3.1.1. Nanoclusters as quantum dots

It has been demonstrated that the inherent non-linear optical response of a dielectric host material, such as glass, polymers, etc., may be enhanced by several orders of magnitude by introducing small semiconductor or metal clusters within the host matrices. Glass researchers have employed various techniques to prepare nanocluster-doped glasses. These nanoclusters are zero-dimensional particles (known as quantum dots) with diameters much smaller than the wavelength of light [19]. Electrons in quantum dots (QDs) are confined between infinite potential barriers [20]. The kinetic energy of such an electron in the case of a sphere of radius a, based on the effective electron mass model (the particle-in-a-box model), is given by

$$E_{n,l} = \frac{h^2}{8\pi^2 m a^2}\,\alpha_{n,l}^2 \tag{9}$$

where m is the effective mass of the electron and $\alpha_{n,l}$ are the zeros of the lth spherical Bessel function. This leads to the decomposition of bulk conduction and valence bands into a set of discrete levels. Thus, the oscillator strengths of many continuous states are concentrated in a few discrete states. The non-linear response of QD materials arises from saturable absorption at the excitonic levels. This effect drastically modifies the quantum states of the electrons and their interaction with applied optical fields; it is referred to as quantum confinement.

Second, when the size of the nanoclusters is much smaller than the wavelength, (λ), of the applied optical field (i.e. for clusters with diameters less than $\lambda/20$), the electric field that acts on and polarizes the free charges of these clusters can be vastly different from the macroscopic field outside the metal clusters in the surrounding medium [21]. This polarization, in turn, modifies the dielectric constant of the composite medium. This effect is called "dielectric or classical confinement". Owing to the difference in dielectric constants between the QDs and the surrounding host material, local field effects arising from dielectric confinement strongly influence the optical properties and can produce major changes in optical response. The local field factor depends on both the shape and the dielectric constant of the particle relative to that of the surrounding medium. Both quantum and dielectric confinement effects alter the susceptibilities of the composite, thereby modifying the linear and non-linear refractive indices and the absorption coefficients.

3.1.1.1. Semiconductor nanocluster–dielectric composite. For semiconductor nanoclusters with a dielectric constant, ε, embedded in a medium of dielectric constant, ε_0, the effective dielectric constant of the composite $\bar{\varepsilon}$ is derived from effective medium theory [22] in the self-consistent field approximation and is expressed as

$$(1-p)\frac{\varepsilon_d - \bar{\varepsilon}}{2\varepsilon + \varepsilon_d} + p\frac{\varepsilon - \bar{\varepsilon}}{2\bar{\varepsilon} + \varepsilon} = 0 \tag{10}$$

where p is the volume fraction of the particles, given by the product of the number density of the particles in the medium and the volume of each particle.

The fields inside, E_{lo}, and outside, E_{ex}, the particles are related by the local field factor, f [23], and are expressed as

$$E_{lo} = fE_{ex} \tag{11}$$

$$f = \left[1 + A\left(\frac{\varepsilon}{\varepsilon_d} - 1\right)\right]^{-1} \tag{12}$$

where A (a geometry-dependent factor) = 1/3 for spherical particles, $1 > A > 1/3$ for oblate spheroidal shapes, $0 < A < 1/3$ for prolate spheroidal shapes.

The electronic structure of a QD depends on the number of atoms constituting the cluster, shape or the

surface area of the cluster and the surrounding environment in the host medium. There is a lower limit to the number of atoms composing the semiconductor QD, if crystalline behaviour of the particle is to be maintained. In practice, QDs are small crystalline particles and are supposed to be chemically identical to the corresponding bulk semiconductor. The most studied semiconductor QD material is CdS which has been embedded in various dielectric materials, such as polymers [24], glasses [25], Langmuir-Blodgett (LB) films [26], etc.

3.1.1.2. Conductive nanocluster–dielectric composite. In a conductive particle–dielectric composite, the field outside the conductive particle is the applied field plus the induced dipole field, while inside the particle the local field drives the optical non-linearity of the medium. In the case of spherical particles much smaller than the wavelength of light, embedded in a dielectric medium with a low-volume fraction p ($p \ll 1$), the effective dielectric constant, $\bar{\varepsilon}$, of such a composite medium in the long wavelength limit, neglecting interactions among particles, is given by [27]

$$\frac{\bar{\varepsilon} - \varepsilon_d}{\bar{\varepsilon} - 2\varepsilon_0} = p\frac{\varepsilon_m - \varepsilon_d}{\varepsilon_m + 2\varepsilon_d} \tag{13}$$

where ε_d, real, is the dielectric constant of the host medium, and ε_m, complex, the dielectric constant of the metal particle [$\varepsilon_m = \varepsilon'_m(\lambda) - i\varepsilon''_m(\lambda)$]. The dielectric constant of a small particle is not necessarily the same as that in a bulk metal due to the quantum size effect. When the volume fraction of the particles $p \ll 1$, one obtains

$$\bar{\varepsilon} = \varepsilon_d + 3p\varepsilon_d\frac{\varepsilon_m - \varepsilon_d}{\varepsilon_m + 2\varepsilon_d} \tag{14}$$

The optical Kerr effect in such a composite is characterized by a change of the effective dielectric constant, $\delta\varepsilon$, resulting from a change $\delta\varepsilon_m$ of the dielectric constant of the metal particles, as given by [28]

$$\delta\bar{\varepsilon} = \left(\frac{3\varepsilon_d}{\varepsilon_m + 2\varepsilon_d}\right)^2 p\delta\varepsilon_m \tag{15}$$

$\delta\varepsilon_m$ is related to the Kerr susceptibility $\chi_m^{(3)}$ of the metal, in the case that only electrons contribute to $\delta\varepsilon_m$, as given by the expression

$$\delta\varepsilon_m = 12\pi\chi_m^{(3)}E_{lo}^2 \tag{16}$$

where E_{lo} is the local field acting on the metal particles and is easily derived by the electrostatic theory. E_{lo} is related to the external field, E_{ex}, as

$$E_{lo} = f_1(\omega)E_{ex} \tag{17}$$

where $f_1(\omega)(= 3\varepsilon_d/(\varepsilon_m + 2\varepsilon_d))$ is the local field enhancement factor describing the first-order susceptibility near or at surface plasmon resonance (SPR) of the metal particles. ω is the angular frequency of the incident light wave. Equation 15 can be written as

$$\delta\bar{\varepsilon} = 12\pi p f_1^4\chi_m^{(3)}E_{ex}^2 \tag{18}$$

and the corresponding polarization is given by

$$P_{NL}^{(3)} = 3pf_1^4\chi_m^{(3)}E_{ex}^3 \tag{19}$$

The local field factor, $f_1(\omega)$, appears in the fourth power and greatly amplifies $P_{NL}^{(3)}$ under SPR conditions [29]. Effective medium theory [30] predicts that the composite susceptibility, $\chi_{eff}^{(3)}$, is related to $\chi_m^{(3)}$ of the metal clusters by

$$\chi_{eff}^{(3)} = pf_1^4\chi_m^{(3)} \tag{20}$$

Equation 20 shows that $\chi_{eff}^{(3)}$ is proportional to the volume fraction and $\chi_m^{(3)}$ of the metal particles and to the fourth power of the local field factor, determined at a frequency close to SPR of the metal particles. Non-linear response is enhanced in such composites from each non-linear region because the optical field can be concentrated in both the interior and the exterior neighbourhoods of the particle. The Kerr susceptibility, $\chi_m^{(3)}$, of the metal clusters includes contributions from intra-band, interband and hot-electron transitions.

(a) Optical absorption of metal nanoclusters in glass. The effect of sample-size on the electronic properties of metals can give insight into the transition from separated metal atoms to bulk metal. A previous study [31] of the optical absorption of small gold particles showed that in one wavelength region, where the optical properties of the metal are determined by interband transitions of the electrons, these properties are unchanged down to particles containing only a few atoms. At longer wavelengths the optical properties of particles below a critical size behave as if they are determined by free electrons, although interband transitions and other unknown processes dominate in larger particles and bulk metal at these wavelengths. In silver, on the other hand, the optical properties of the bulk metal appear to be determined entirely by free electrons in the visible region [32].

If the optical properties of a metal are determined by free electrons, the following equation is valid for its dielectric constant under the conditions of interest here.

$$\varepsilon_m = \varepsilon_0 - \left[\frac{4\pi N_e e^2}{(2\pi c)^2 m}\right]\lambda^2 - i\left[\frac{4\pi N_e^2 e^2}{(2\pi c)^3 m^2\sigma}\right]\lambda^3 \tag{21}$$

where ε_0 is the frequency-independent part of ε_m, σ is the d.c. electrical conductivity, λ is the wavelength, c is the velocity of light, and N_e, m and e are the number density, mass and charge of the free electrons, respectively.

Fig. 1 shows the plots of the real and imaginary parts of ε_m for silver particles in glass, as measured by Otter [33], as a function of wavelength squared. The ε'_m values are proportional to λ^2 above a wavelength of about 0.40 μm; substantial deviations appear only below about 0.35 μm. Extrapolation of ε'_m to shorter wavelengths was based on the functional dependence of ε'_m upon λ found by Ehrenreich and Philipp [34] at these wavelengths. The ε''_m values are proportional to λ^3, except for a few scattered points above about 0.46 μm; below this wavelength, the values of ε''_m increase sharply, presumably because of the onset of

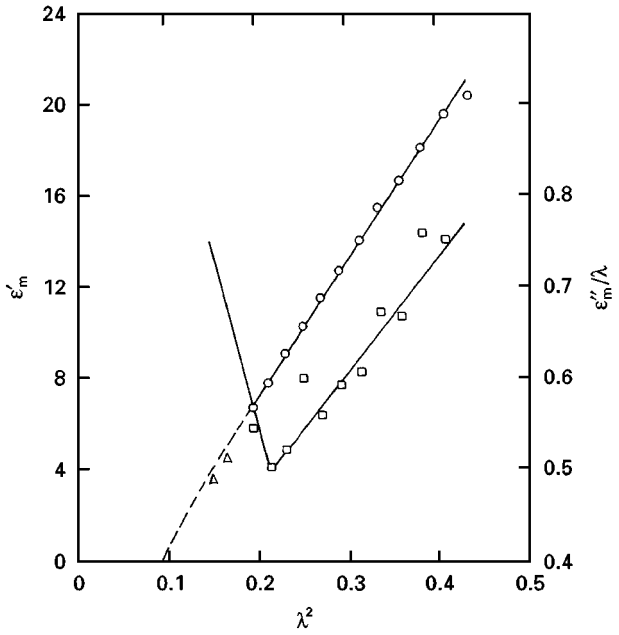

Figure 1 Optical properties of silver, as measured by Otter [33]. (○) ε'_m, (□) ε''_m/λ, (△) ε'_m from absorption bands of particles.

interband transitions [32]. The line for ε''_m/λ at shorter wavelengths was estimated from the measurements of Schulze [35]. The slope of the ε''_m/λ versus λ^2 line, drawn in Fig. 1, in the free-electron region agrees with Equation 21, using the bulk d.c. conductivity for σ.

The silver particles were formed [32] in a glass of composition (in weight per cent): 71.5% SiO_2, 23.5% Na_2O, 4% Al_2O_3, 1% ZnO, 0.02% CeO_2 and 0.002% Ag. The glass was held molten for several hours at 1400 °C, and then cooled rapidly to room temperature to prevent reduction and precipitation of the silver. Silver particles were nucleated by irradiation of glass samples at room temperature with ultraviolet light, and grown by heating at higher temperatures, usually at 580 °C. The optical absorption measurements were made for these silver particles in glass [32] at room temperature as well as at higher temperatures. A sharp absorption band was found to appear with a peak at 0.406 μm only at high temperature and the glass became yellow. With higher annealing temperatures the band was found to become sharper but the peak position remained fixed. Without silver in the glass no such band was found to develop. A similar band was found by Yokota and Shimizu [36] for a silver–glass.

The optical absorption coefficient, α, of a collection of uniform spheres, very small compared to the wavelength, λ, of light and embedded in a medium of refractive index n_d, is well described by the Mie scattering theory [37] in the electric dipole approximation and is given by

$$\alpha = p\,\frac{18\pi n_d^3\,\varepsilon''_m}{\lambda\,[(\varepsilon'_m + 2n_d^2)^2 + \varepsilon''_m]} \tag{22}$$

Equation 22 can be approximated as follows

$$\alpha \approx p\,\frac{\omega}{cn_d}\,|f_1^2|\,\varepsilon''_m \tag{23}$$

where $\varepsilon_m(\lambda)$ $[= \varepsilon'_m(\lambda) - i\varepsilon''_m(\lambda)]$ is the frequency-dependent dielectric constant of the metal spheres, and p is the volume fraction of the spheres in the glass. The particles must be far enough apart so that there is no multiple scattering and they scatter independently. The critical (upper-limit) diameter of the sphere for the present conditions is roughly 10 nm, as calculated from the more complete equation of Mie [37]. The absorption coefficient has a maximum at the surface plasmon resonance frequency, ω_{sp}, where $\varepsilon'_m + 2n_d^2 = 0$. (Surface plasmons are the quanta of surface charge density oscillations. The same terminology is used for collective oscillations in the electron density at the surface of a metal. From a macroscopic electrodynamic point of view, surface plasmons are a type of surface wave, i.e. waves that propagate along metal surfaces and which decay in a normal direction from the surfaces.) The surface plasmon resonance frequency depends implicitly on the metal-particle size through the dielectric constant of the metal particles which is modified if the mean free path of the conduction electrons exceeds the cluster size [36]. Equation 22 shows that the plasmon band has a peak at $\varepsilon'_m = -2n_d^2$; the peak wavelength of the band depends on the dielectric constants of the matrix and the metal particles.

If the optical properties, shown in Fig. 1, are substituted into Equation 22, a band with maximum absorption at 0.396 μm results. Therefore, it seems reasonable to attribute the band found experimentally to very small, spherical silver particles in the glass. If the particles were not spherical (or equiaxial), the absorption band would be at longer wavelengths and would gradually shift to lower wavelengths as the particles became more spherical.

The width of the calculated absorption band was found to be about ten times smaller than the narrowest band measured in the study of Doremus [32]. This discrepancy can be understood by considering the effect of the particle size upon the mean free path of the electrons, because the particles are much smaller than the mean free path of electrons in bulk silver (~ 52 nm) at room temperature.

If the complete expression for the dielectric constant of a metal, when it is determined by free electrons, is substituted in Equation 22, the result is as follows [38]

$$\alpha = \frac{9\pi p n_d^3 c}{\sigma}\,\frac{\lambda^2}{(\lambda_m^2 - \lambda^2)^2 + \lambda^2\lambda_m^4/\lambda_a^2} \tag{24}$$

where $\lambda_m = \lambda_c(\varepsilon_0 + 2n_d^2)^{1/2}$ is the wavelength at which the maximum absorption takes place. $\lambda_c = (2\pi c)^2 m/4\pi N_e\varepsilon_m^2$ and $\lambda_a = 2\lambda_c^2\sigma/c$. Equation 24 gives a band of Lorentzian shape: if the band is narrow, its width, w, at half maximum absorption (FWHM) is λ_m^2/λ_a and is given by

$$\begin{aligned} \omega &= \lambda_m^2/\lambda_a \\ &= (\varepsilon_0 + 2n_d^2)c/2\sigma \end{aligned} \tag{25}$$

The d.c. conductivity, σ, is given by [38]

$$\sigma = (N_e e^2 R)/mu_F \tag{26}$$

where R is the particle radius, $u_F[=(2E_F/m)^{1/2}]$ is the electron velocity at the Fermi energy $E_F(=(3n/8\pi)^{2/3}(h^2/2m))$, and N_e is the number of electrons per unit volume.

Therefore, the experimental result of constant band position is reasonable, because λ_m does not depend upon the conductivity, σ, which is determined by the mean free path of the electrons and therefore, upon the particle size. Alternatively, Equation 25 shows that the dependence of bandwidth upon particle size, i.e. $w \propto 1/R$, as obtained from Equations 25 and 26, results from the changing mean free path of the electrons. In Fig. 2, the experimentally measured absorption band for silver particles of about 10 nm diameter, suspended in glass, is compared to that calculated from Equation 24, using the measured λ_m and bandwidth [32]. The agreement between these curves confirms that the absorption results from the free electrons in the silver particles. The slight increase in absorption at lower wavelengths probably results from the ultraviolet irradiation of the cerium present in the glass matrix [32].

The area under the absorption band is proportional to the total amount of silver in the particles. The average radius of the particles is proportional to the cube root of this area as long as the size distribution of the particles is narrow. To compare Equation 25 quantitatively with the experimental measurements of the bandwidth, it is necessary to know the size of the particles. Above a certain particle size, the absorption band begins to shift to longer wavelengths because additional magnetic-dipole terms appear in Equation 22 for larger radii particles. This critical diameter for the present conditions is roughly 10 nm, as calculated from the more complete equations of Mie [37]. The d.c. conductivity for a silver particle of radius 5 nm, as calculated from Equation 26, is 6.07×10^{16} (taking $N_e e^2/m = 1.70 \times (10)^{31}$ from Otter's data and $u_F = 1.40 \times 10^6\ \mathrm{m\,s^{-1}}$). Using this value of σ, together with $n_d = 1.5$ (for glass) and $\varepsilon_0 = 4.9$, in Equation 25 gives a bandwidth of 22.5 nm which is close to the experimental value (Fig. 2). Therefore, within the error of estimating the particle size, the bandwidth calculation follows the simple assumption that the mean free path of the electron is equal to the particle size. Fig. 3 shows the calculated Mie extinction coefficient of silver colloids of various radii as a function of wavelength. Constancy in the band position for various cluster sizes and the diminishing bandwidth for increasing cluster size (up to the critical size of 10 nm diameter), as seen in Fig. 3, agree with the expected results obtained from Equations 25 and 26.

Fig. 4 shows the optical absorption spectrum for gold-implanted SiO_2 samples [39]. The peak at the calculated value of 2.4 eV is due to the surface plasmon resonance (SPR) of gold nanoclusters occurring at that incident energy. The cluster diameter, estimated for the "as-implanted" sample, is < 5 nm while

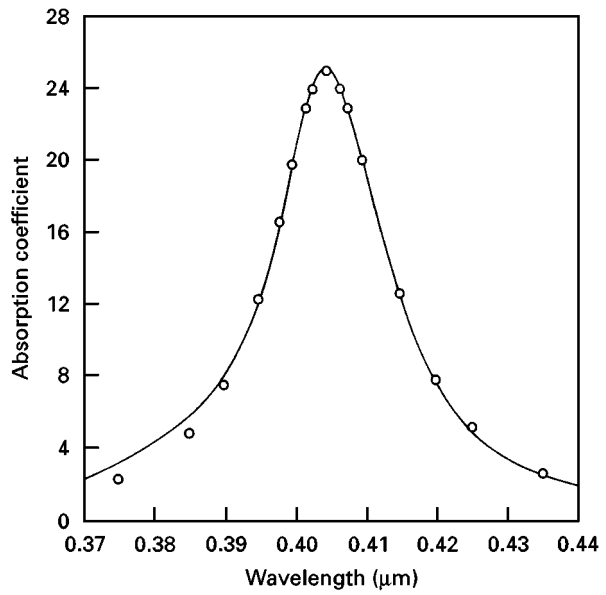

Figure 2 (○) Measured and (—) calculated absorption band for silver particles of about 10 nm diameter, suspended in glass [32].

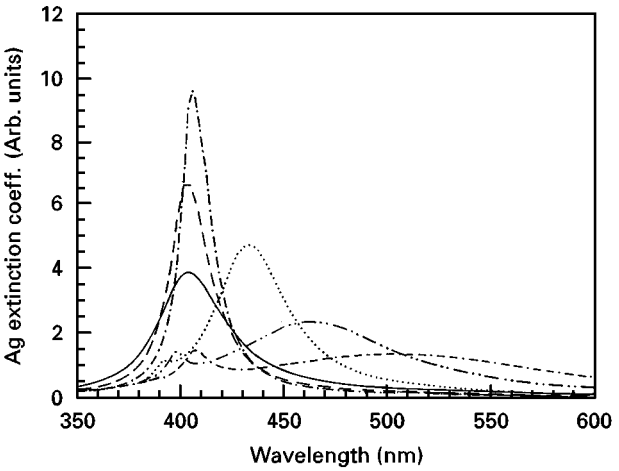

Figure 3 Mie extinction coefficient of silver colloids of various radii as a function of wavelength of the incident light. R (nm): (—) 2.5, (– – –) 5, (—·—) 10, (···) 25, (—··—) 35, (– –·– –) 45.

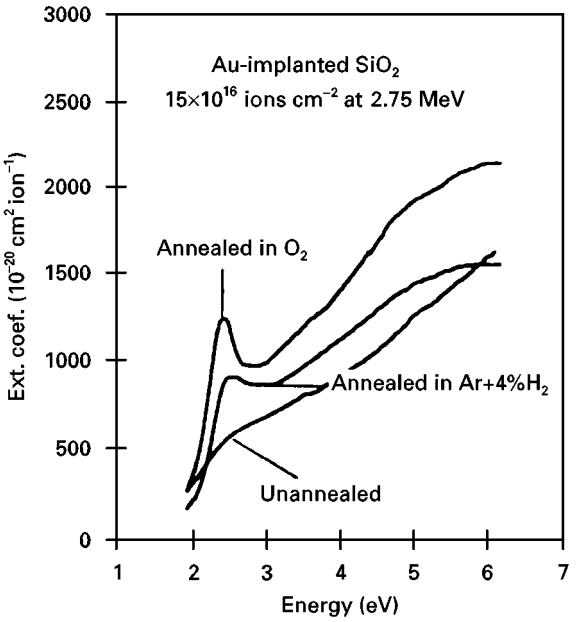

Figure 4 Optical absorption spectra of three samples: as-implanted, annealed in oxygen at 900 °C, and annealed in a mixture of argon and 4% H_2 at 1100 °C [39].

that in the implanted samples clusters have diameters in the 5–30 nm range. The roughly linear increase in absorption between 2 and 4 eV is consistent with the $1/\lambda$ dependence in Equation 22. The overall increase in absorption upon heat treatment could be due to an increase in volume fraction of gold colloids contributing both to the SPR and to the $1/\lambda$ background term. Clusters smaller than 1 nm in size do not contribute to the SPR absorption peak, whereas the SPR peak becomes more distinct and increases in amplitude with increasing cluster size.

The electronic non-linearity in the case of small metal particles may originate from three processes.

(i) The intraband transition of electrons in the conduction band. The intraband electron contribution vanishes in the bulk. The free electrons (i.e. the conduction electrons) show non-linear behaviour in particles due to the quantum-size effect [40].

(ii) The saturation of the interband transition, which occurs between the *d*-levels and the conduction band. This process is a resonant and size-independent one, corresponding to the saturation of the two-level transition between the bands. The saturation leads to a modification of the linear properties [41].

(iii) The creation of hot photo-excited electrons due to the strong absorption near the surface plasmon resonance, which, in turn, depends on the particle size, leading to a change in the Fermi–Dirac distribution and hence in the interband transition [42].

Of these three contributions, the first one is strongly size dependent. The size dependence occurs because the nearly free-electron wave functions characteristic of the bulk metal are modified by confining the electrons to a small volume with dimensions much smaller than the characteristic electron mean free path in the bulk metal. Because the Debye screening length for electrons in the clusters is very short (~ 0.1 nm), while the penetration of the electron wave functions into the surrounding silica is necessarily extremely small, it is reasonable to treat the valence or conduction electrons of the metal nanoclusters as independent particles confined in a spherical potential well. In addition, the level spacing of the electronic states is so large, even at cluster sizes as big as 10–12 nm in diameter, that the optical transitions may be viewed as transitions between pairs of discrete levels. These two facts, taken together, allow the susceptibilities to be calculated, as if one were dealing with independent particles in the two-level approximation. The confinement of the conduction electrons, which can be classically described in terms of limited mean free path gives rise to an expression for $\chi^{(3)}$ varying roughly as $1/R^3$, if R is the radius of the metal sphere. Therefore, we expect to see this term contributing primarily for the smaller nanoclusters.

For metal particles embedded in a dielectric medium, the absorption becomes a limiting factor in raising the volume fraction content. The enhancement of non-linear response is accompanied by an increase of absorbance. In the vicinity of the surface plasmon resonance, such composite materials have $\chi^{(3)}$ of the order of 10^{-8} e.s.u. obtained from DFWM experiments, with response times of the order of picoseconds [30]. The surface plasmon resonance frequency, ω_{sp}, can be shifted by varying the shape of the metal particle and for a mixture of particles of various shapes; the total $\chi^{(3)}$ is the sum of contributions from each shape weighted by its volume fraction. The control of the shape, size of the particle and the choice of the dielectric host medium are important for the optimization of NLO properties of the composite.

3.1.1.3. Ion implantation and synthesis of nanoclusters in glasses. Because the incorporation of semiconductor or metallic nanoclusters in dielectrics enhances the third-order optical non-linearity, it would be desirable to use a method in which the non-linearity could be confined to specific patterned regions in order to provide effective designs of integrated optical devices. This clearly calls for the use of ion implantation. Although several other methods, such as ion-exchange [43], sol–gel [44], electrolytic colouration, etc., also exist for introducing the metal into the insulating substrates, the ion implantation has the advantage of being a generally applicable process; it can be performed at an ambient temperature; it has no side-diffusion problems. Moreover, it offers an accurate control of the total number of ions being added to the target and a predictable depth distribution in the target matrix determined by the incident ion-beam energy. Ion implantation in glassy structures yields in the precipitation of metal colloids at a reasonably higher local concentration because of the large specific volume and more open structure of the glassy state relative to that of the crystalline counterpart.

Nanocluster formation in metal-ion implanted silica and glasses has been studied by using different techniques. Optical absorption measurements and transmission electron microscopy (TEM) give information on cluster shape, size and crystalline state. Cross-sectional TEM measurements give the details of colloid size distribution as a function of depth [45]. Rutherford backscattering spectroscopy (RBS), and secondary ion mass spectrometry (SIMS) can be used to obtain the depth distribution of the implanted species. X-ray photoelectron spectroscopy (XPS) and Auger electron spectroscopy (AES) determine the chemical state of the implanted ions. Degenerate four-wave mixing (DFWM) [28] and *Z*-scan [46] methods have been used for measurements of $\chi^{(3)}$ of the metal-doped glasses. Fig. 5 shows the RBS spectra of copper-implanted silica, showing the bimodal distribution of the concentration of copper atoms as a function of depth for two different ion fluences [21]. The height of the larger peak is approximately twice that of the smaller one and located nearer to the surface. The bimodal distribution has also been observed in case of other implants in silica.

Ricard *et al.* [28] were the first to measure the non-linear properties of such colloids (silver, gold) in bulk silica and other workers [39] extended these measurements. The optical Kerr susceptibility was found to be two to three orders of magnitude greater than that of the bulk metals. The non-linear index, n_2, of 160 keV copper-implanted silica, at a fluence of

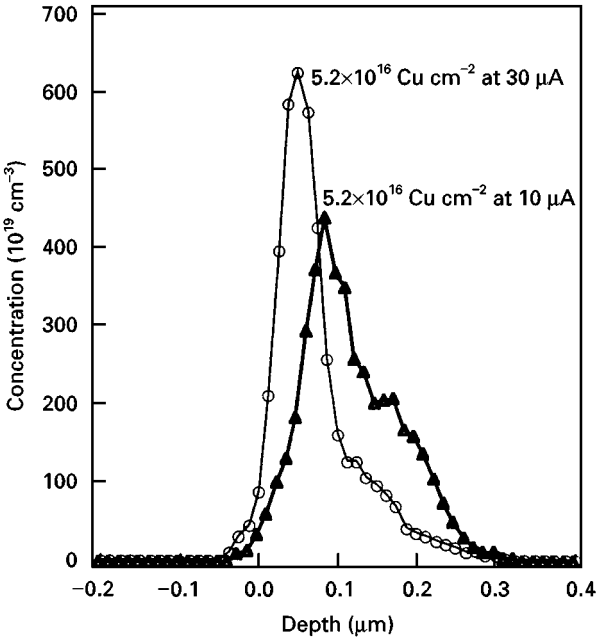

Figure 5 RBS spectra of a Cu^+-implanted silica for two different ion doses, showing the distribution (bimodal) of copper atoms as a function of depth. The larger peak is approximately twice the size of the smaller one and located nearer to the surface [21].

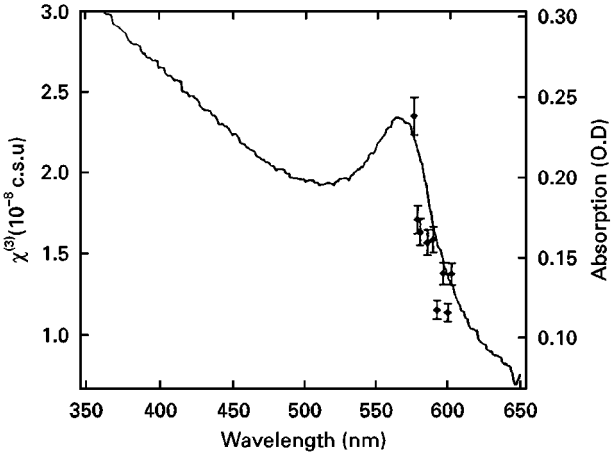

Figure 6 $\chi^{(3)}$ and absorption coefficient of 160 keV, 10^{17} ions cm^{-2} copper-implanted silica composite as a function of wavelength. The apparent maximum in $\chi^{(3)}$ near 2.2 eV suggests that the excitation of the SPR contributes to the third-order non-linear response of the composite [47].

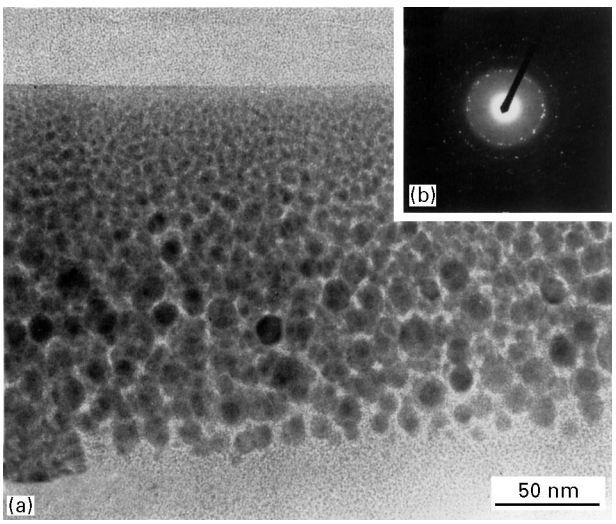

Figure 7 (a) Transmission electron micrograph of the microstructure in a Sn^+-implanted silica–glass, showing the precipitation of spherical nanoclusters of tin in the host matrix [52]. (b) The electron diffraction pattern of the cross-section of the implanted sample.

10^{17} ions cm^{-2}, was determined [47] using the *Z*-scan method and was found to be around 4×10^{-14} m^2 W^{-1}. Fig. 6 shows $\chi^{(3)}$ of such a composite as a function of wavelength near the 2.2 eV peak in the optical absorption spectrum and the magnitude of $\chi^{(3)}$ is found to be $\sim 10^{-8}$ e.s.u. The apparent maximum in $\chi^{(3)}$ at SPR suggests that the excitation of the surface plasmon resonance contributes to the non-linear response in the composite. The maximum value of $\chi^{(3)}$ at maximum optical absorption is also understood from Equations 20 and 23, taken together. The main contribution to the electronic non-linearity near SPR in this case is attributed to photoexcitation of electrons in the conduction band.

More recently, the formation of various metal colloids (copper, silver, gold, lead, tin, iron, phosphorus, etc.) in silica glasses by ion implantation under various conditions and measurements of $\chi^{(3)}$ values in these cases, have been reported [48–52]. The highest value of $\chi^{(3)}$ (3×10^{-6} e.s.u.) was obtained, so far, for tin-implanted (2×10^{17} ions cm^{-2} dose) silica glass [52] at a wavelength of 500 nm; corresponding to SPR of tin. Metallic tin microcrystallites of diameters in the range 4–20 nm, distributed in the region between 10 and 200 nm from the surface, were observed by TEM. Figs 7 and 8 show the TEM image and the X-ray diffraction (XRD) pattern of the microstructures, respectively, in such a composite [52]. The implanted ions, as shown in Fig. 7, form spherical nanoclusters. From the magnified image of Fig. 7 (not shown), each particle was seen to be of a single domain. The inset in Fig. 7 shows the electron diffraction pattern of the cross-section of the implanted sample. The crystallinity of the nanoclusters is evidenced by the peaks in XRD (Fig. 8). All the XRD peaks are identified as those of metallic tin crystallites and relative peak intensities confirm that there is no evidence of preferential orientation of the microcrystallites. These results indicate that almost all the particles are crystallized, which is consistent with the fact that tin crystallizes below room temperature. From the RBS measurements of such a composite [52], an average volume fraction of the microcrystallites was also estimated and was found to be 28%. The measured non-linear refractive indices ($\sim 10^{-6}$ e.s.u.) for these tin microcrystallite-doped glass composites compare well to that of II–VI semiconductor-doped glasses and are much larger than that of colloidal melt-glasses. For a metal cluster with a cubic symmetry, the fourth-rank tensor $\chi^{(3)}$ has four independent components. Of these, $\chi^{(3)}_{xxxx}$ includes contributions from both thermal and electronic processes. The $\chi^{(3)}_{xxyy}$ component, on the other hand, is sensitive only to electronic processes. The enhancement in the electronic component of $\chi^{(3)}$

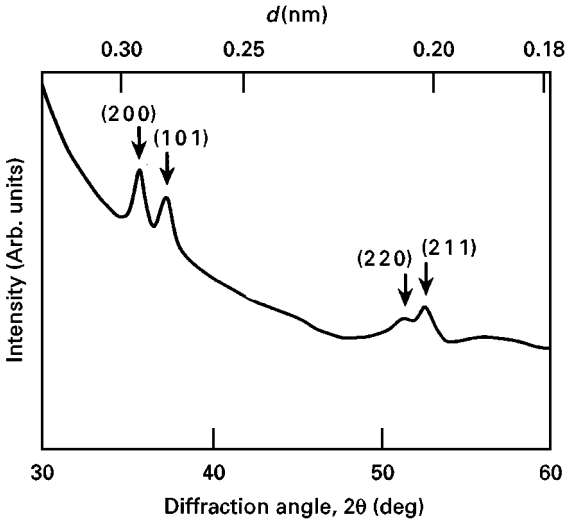

Figure 8 The X-ray diffraction (XRD) pattern of the microstructure of the same sample, as discussed in Fig. 8. The crystallinity of the nanoclusters is evinced by the peaks.

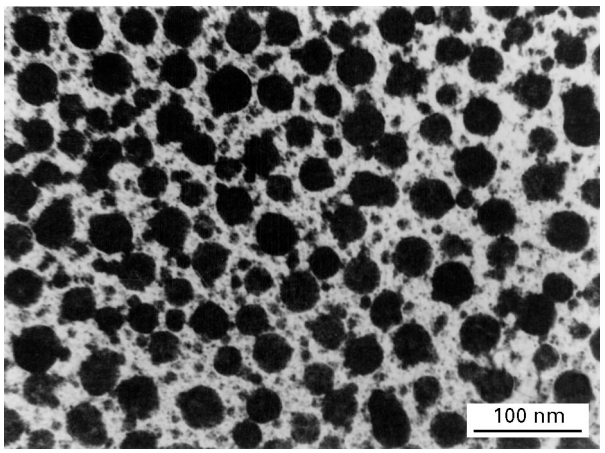

Figure 9 Transmission electron micrograph of a sequentially Ag^+- and Cu^+-implanted silica. Smaller clusters exist in the near-surface region while the larger clusters are located deeper in the implanted region [53].

due to the increased volume fraction ($\sim$30%) of the nanoclusters in the composite is obviously an important consideration from the point of view of non-linear optics, but achieving such a high concentration of dopants is a non-trivial materials problem. A volume fraction of such magnitude, obtainable by ion implantation only, cannot be made in a melt-glass because of the constraints of chemical and thermodynamic equilibrium. This points to one major advantage of ion-implantation as a technique for synthesizing nanocluster–glass composites. Fig. 9 shows a transmission electron micrograph of the sequentially silver and copper implanted silica [53]. The implantation energies (300 and 160 keV for silver and copper ions, respectively) were such that the depth of implantation for each species should overlap. As seen in this figure, smaller clusters exist in the near-surface region while the large clusters are located deeper in the implanted region.

3.1.1.4. Magnitude and temporal response of $\chi^{(3)}$ in nanocluster–glass composites. Progress in non-linear optical materials is the key to creating functional photonic devices for optical communications, sensing and computing. Understanding the correlation between materials processing and optical non-linearities is critical to the development of advanced non-linear materials for photonic devices. Optical switching at tetrahertz frequencies requires non-linear optical materials with the following properties: picosecond or shorter response times, low-power switching threshold, high thermal stability, low two-photon absorption, wavelength tunability, and a high threshold for laser-induced damage.

There are many materials with high third-order non-linearities, although only a large value of $\chi^{(3)}$ is not sufficient. The key issue for light-wave technology is to optimize performance of third-order materials in real device geometries under realistic operating conditions. Moreover, the long-term mechanical, thermal and optical stability of potential waveguide devices can only be tested accurately in actual device geometries. Thus the results achieved with metal nanocluster composites made by ion implantation are significant because of their potential for making a high-performance non-linear material using an established ion-implantation-based waveguide fabrication technology [53].

Fig. 10 compares a variety of electronic and photonic materials with respect to two crucial device parameters of switching energy and switching speed [54]. As shown in the hatched area, nanocluster composites of $Au:SiO_2$ and $Cu:SiO_2$ have faster switching speeds than any material, except para-toluene sulphonate (PTS), which, however, suffers from long-term photochemical damage. The shaded area in the figure indicates the range of switching energies projected from theoretical estimates for metal nanocluster composites.

While no single material exhibits all the characteristics of an ideal optical switch, metal nanocluster composites do seem to offer an attractive combination. However, both for the demonstration of device potential and for studying optical physics in these

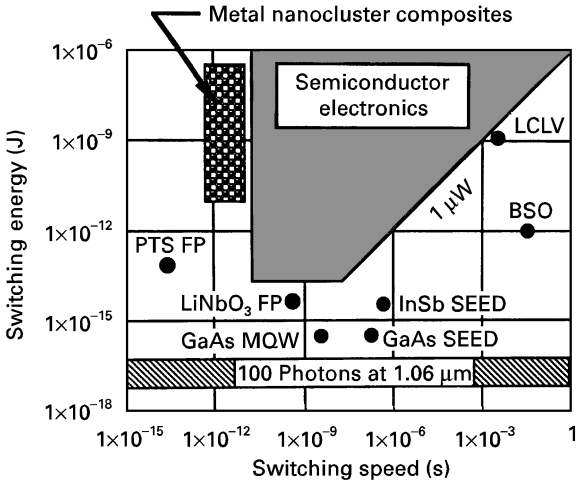

Figure 10 Comparison of a variety of electronic and photonic materials with respect to switching energy and switching speed [54].

interesting non-linear materials, it may be advantageous to carry out the non-linear studies in actual waveguide geometries. For example, because two-photon absorption, which is proportional to the imaginary part of $\chi^{(3)}$, arising not only from the clusters but also from the defects created by ion implantation, severely limits all-optical device performances, a fundamental understanding of its origin and relation to size, shape and density of the clusters in the waveguide is crucial. In optical switching devices and waveguide, a key-parameter is the non-linear index of refraction, proportional to the real part of $\chi^{(3)}$.

Measurements of the magnitude and the temporal response characteristics of $\chi^{(3)}$ are the most important part of the experiments. One can measure $\chi^{(3)}$ at wavelengths both on and off the SPR by forward DFWM in the geometry of Fig. 11 [21]. In a guided wave geometry, it is possible to use a CW mode locked laser for four-wave mixing studies with counter-propagating pump-beams. In DFWM configuration, three different light fields, E_1, E_2 and E_3, of the same frequency are incident on the non-linear optical material to produce a fourth beam, E_4. It is also called phase conjugation or real-time holography. Two different types of volume holograms, i.e. reflection and transmission holograms can be constructed. In either type, the third beam is used as the reading beam and the fourth one is the result of the diffraction of the hologram, making E_4 conjugate to E_3. The third-order NLO susceptibility is given by [55]

$$\chi^{(3)} = \frac{8c^2 n_d^2 \varepsilon_0 \alpha \eta^{1/2}}{3\omega I_1 (1 - T)} \tag{27}$$

where n_d and α are linear refractive index of the host matrix and absorption coefficient of the nanocluster–glass composite, respectively, both measured at the same frequency, ω, of the optical signal close to the SPR of the composite, I_1 is the pump intensity, c is the velocity of light in vacuum, T is the transmittance of the medium at ω, and η is the diffraction efficiency of the holographic grating.

DFWM experiments also give important information on the switching speed. $\chi^{(3)}$ for gold nanoclusters in glass was measured by Magruder *et al.* [39] by DFWM using a mode-locked Q-switched, frequency-doubled Nd:YAG laser at a wavelength of 532 nm with a pulse repetition frequency of 10 Hz and a nominal pulse width of 35 ± 5 ps. This wavelength is near the SPR of gold (530 nm). The two forward-going pump-beams and a weak probe-beam were arranged to intersect in the composite-layer containing the metal clusters. The probe was delayed with respect to the two pump beams using a computer-controlled optical delay line. The pump and probe beams interacted coherently via the third-order non-linear susceptibility to produce a phase-conjugated signal, detected in a photomultiplier. Identical measurements were carried out on unimplanted samples; no measurable DFWM signal was observed. Fig. 12 shows the intensity of the phase-conjugated signal as a function of pump probe delay time [39]. The symmetric shape of the time spectrum indicates that the third-order response is no longer than that of the pulse width (~ 35 ps). The measured values of $\chi^{(3)}$ were found to be 1.0×10^{-10} and 1.7×10^{-10} e.s.u. for this nanocluster composite layer without and with heat treatment, respectively.

For gold nanocluster–glass composite, with $n_2 = 0.0395\chi^{(3)} n_d^2$, the figure-of-merit F for waveguide devices ($F = \Delta n_{sat}/\tau\alpha$ where $\Delta n_{sat} = n_2 I_{sat}$) ~ 0.04 [39], which is an order of magnitude smaller than Cd_xSe_{1-x} quantum-dots in glass. However, the figure-of-merit can be made more attractive by shifting the wavelength slightly off the surface plasmon resonance [47] or by choosing a proper ion–target combination.

In a waveguide, planar or channel or fibre, the light beam is confined in one- or two-dimensions to values of the order of the wavelength of light. The propagation lengths are typically millimetres to centimetres in integrated-optics waveguides and metres to kilometres in fibres. Taking into account the non-linearity

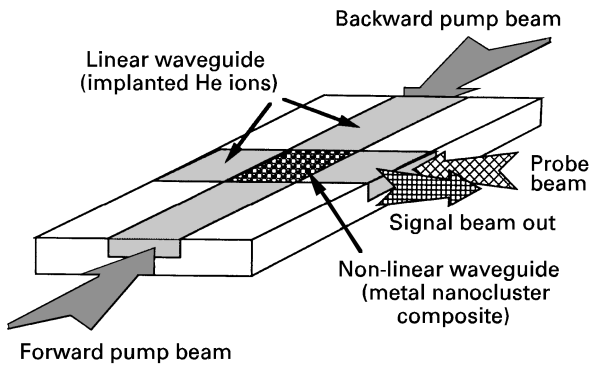

Figure 11 Schematic drawing of a cross-channel waveguide made by a two-stage ion-implantation process. The light guide is provided by a helium-implanted channel; the non-linear element is made by implanting a section at the centre of the cross with noble metal ions. Such a device would be appropriate for a four-wave mixing process [21].

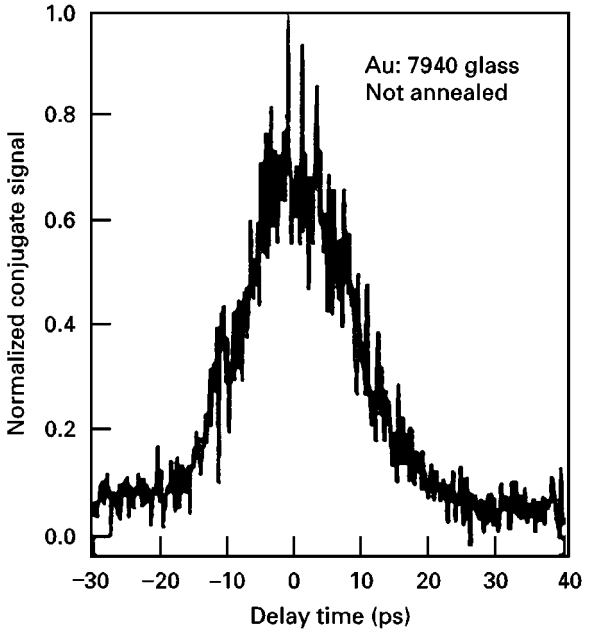

Figure 12 Intensity of the phase-conjugated beam in a DFWM measurement with cross-polarized pump-probe configuration as a function of pump-probe time in picoseconds [39].

of relaxation time, we can see from the considerations of the figure-of-merit that organics and glasses are more suitable for all-optical processing applications. For a given switching power, the smaller non-linearity can be compensated by longer interaction length, L, with the limit A/α, where A is the acceptable loss and α is the attenuation coefficient [56]. As glasses have the lowest α and n_2, they can be used as fibres, whereas organics have reasonably low attenuation and relatively high non-linearity, and therefore they are potentially useful for channelled integrated-optics applications.

All-optical devices, however, require some kind of laser source as well as non-linear optical elements, in combination. Recent research works demonstrating harmonic generations in ion-implanted single crystals like $KNbO_3$ [57], laser actions in systems like chromium-doped $LiNbO_3$ [58], rare-earth element (erbium)-doped crystals and glassy materials [59, 60], etc., seem to be quite encouraging in this respect as the possible coupling of such laser light sources with non-linear optical waveguides can lead to success in realizing complete photonic devices.

4. Conclusion

The main impediment to the practical exploitation of non-linear optics is the difficulty in understanding and developing materials that can be engineered to match device needs. New device concepts and materials developments are two key factors for future success. The criteria used to define the figure of merit are conditional and so the selection of material is crucial. The best material for one application may be the worst for another. For example, materials possessing large photorefractive effect and optical Kerr effect are useful for optical switching. As these two effects are competing processes for harmonic generation, the corresponding materials are excellent for optical switching but poor for harmonic generation, whereas the relatively long relaxation times of semiconductors are disadvantageous for serial optical switching.

The enhanced non-linear optical properties of metal colloids in silica glasses, obtained by ion implantation and their fast temporal responses (i.e. in sub-picosecond time domain) suggest that the ion-implantation technique plays an important role in the production of non-linear photonic materials. Thus, from these recent achievements, together with remarkable advances in semiconductor materials fabrication technology, one can see the movement of optics into the electronic switching fabric and the beginning of hybridization between electronic and photonic switching technologies.

Acknowledgements

The author thanks Professor Paolo Mazzoldi, Physics Department, Padova University, Italy, for introducing him to this subject, Prof. G. Battaglin, Dr F. Caccavale, Dr F. Gonella and others of the same centre, and Dr G. W. Arnold, Sandia National Laboratories, New Mexico, USA, for many valuable discussions on this subject.

References

1. P. W. SMITH, *Bell Svs. Tech. J.* **61** (1982) 1975.
2. S. R. FRIBERG and P. W. SMITH, *IEEE J. Quantum Electron.* **QE-23** (1987) 2089.
3. E. M. VOGEL, *J. Am. Ceram. Soc.* **72** (1989) 719.
4. N. BLOEMBERGEN, "Nonlinear Optics" (W. A. Benjamin, NY, 1965).
5. A. AL-SAIDI and R. G. HARRISON, *Appl. Phys. B* **36** (1985) 17.
6. P. D. MASON, D. J. JACKSON and E. K. GORTON, *Opt. Commun.* **110** (1994) 163.
7. D. R. SUHRE, *Appl. Phys. B* **52** (1991) 367.
8. M. HAGEMANN and H. J. WEBER, *Appl. Phys. A* **63** (1996) 67.
9. M. BASS, P. A. FRANKEN, A. E. HILL, C. W. PETERS and G. WEINREICH, *Phys. Rev. Lett.* **8** (1962) 18.
10. I. D. ABELLA, *ibid.* **9** (1962) 453.
11. V. MIZRAHI, K. W. DELONG, G. I. STEGEMAN, M. A. SAIFI and M. J. ANDREJCO, *Opt. Lett.* **14** (1989) 1140.
12. M. J. WEBER, D. MILAN and W. L. SMITH, *Opt. Eng.* **17** (1978) 463.
13. D. S. CHEMLA, D. A. B. MILLER, P. W. SMITH, A. C. GOSSARD and W. WIEGMAN, *IEEE J. Quantum Electron.* **QE-20** (1984) 265.
14. N. L. BOLING, A. G. GLASS and A. OWYOUNG, *ibid.* **QE-14** (1978) 601.
15. R. ADAIR, L. L. CHASE, and S. A. PAYNE, *J. Opt. Soc. Am. B: Opt Phys.* **4** (1987) 875.
16. E. M. VOGEL, M. J. WEBER and D. M. KROL, *Phys. Chem. Glasses* **32** (1991) 231.
17. G. I. STEGEMAN, R. H. STOLEN, *J. Opt. Soc. Am. B* **6** (1989) 652.
18. S. R. FRIBERG, Y. SILBERBERG, M. K. OLIVER, M. J. ANDEREJCO, M. A. SAIFI and P. W. SMITH, *Appl. Phys. Lett.* **51** (1987) 15.
19. D. S. CHEMLA and D. A. B. MILLER, *J. Opt. Soc. Am. B* **2** (1985) 1155.
20. A. KAWABATA and R. KUBO, *J. Phys. Soc. Jpn* **21** (1966) 1765.
21. R. F. HAGLUND Jr, L. YANG, R. H. MAGRUDER III, C. W. WHITE, R. A. ZUHR, LINA YANG, R. DORSINVILLE and R. R. ALFANO, *Nucl. Instrum. Meth. B* **91** (1994) 493.
22. R. LANDAUER, in "Electrical Transport and Optical Properties of Inhomogeneous Media," edited by J. C. Garland and D. B. Tanner (American Institute of Physics, New York, 1978) p. 2.
23. Y. Q. LI, C. C. SUNG, R. INGUVA, C. M. BOWDEN, *J. Opt. Soc. Am. B* **6** (1989) 814.
24. Y. WANG and W. MAHLER, *Opt. Commun.* **61** (1987) 233.
25. A. I. EKMOV, A. L. ALFROS and A. A. ONUSHCHENKO, *Sol. State. Commun.* **56** (1985) 921.
26. C. LIU and A. BARD, *J. Chem. Phys.* **93** (1989) 3232.
27. D. K. HLE, *J. Mater. Sci.* **11** (1976) 2105.
28. D. RICARD, P. ROUSSOGNAL and C. FLYTZANIS, *Opt. Lett.* **10** (1985) 511.
29. J. A. ARMSTRONG, N. BLOEMBERGEN, J. DUCUING and P. PERSHAN, *Phys. Rev.* **127** (1962) 1918.
30. J. W. HAUS, N. KALYANIWALLA, R. INGUVA and C. M. BOWDEN, *J. Opt. Soc. Am. B* **6** (1989) 797.
31. R. H. DOREMUS, *J. Chem. Phys.* **40** (1964) 2389.
32. *Idem*, *ibid.* **42** (1965) 414.
33. W. OTTER, *Z. Physik* **161** (1961) 163.
34. H. EHRENREICH and H. R. PHILIPP, *Phys. Rev.* **128** (1962) 1622.
35. L. G. SCHULZE, *J. Opt. Soc. Am.* **44** (1954) 357.
36. R. YOKOTA and K. SHIMIZU, *J. Phys. Soc. Jpn* **12** (1957) 833.
37. G. MIE, *Ann. Phys.* **25** (1908) 377.
38. W. J. DOYLE, *Phys. Rev.* **111** (1958) 1067.
39. R. H. MAGRUDER III, L. YANG, R. F. HAGLUND Jr, C. W. WHITE, LINA YANG, R. DORSINVILLE and R. R. ALFANO, *Appl. Phys. Lett.* **62** (1993) 1730.
40. F. HACHE, D. RICARD and C. FLYTZANIS, *J. Opt. Soc. Am. B* **3** (1986) 1647.

41. N. E. CHRISTENSEN, B. O. SERAPHIN, *Phys. Rev. B* **4** (1971) 3321.
42. F. HACHE, D. RICARD, C. FLYTZANIS and U. KREIBIG, *Appl. Phys. A* **47** (1988) 347.
43. G. BATTAGLIN, R. POLLONI, G. De MARCHI, F. CACCAVALE, F. GONELLA, G. MATTEI, P. MAZZOLDI, A. QUARANTA, F. SPIZZO, G. DE and R. F. HAGLUND Jr, in "Proceedings of the International Conference on Fibre Optics and Photonics, Photonics-96", edited by J. P. Raina and P. R. Vaya (Tata McGraw-Hill Publishing Co., New Delhi) India, p. 36.
44. M. MENNIG, M. SCHMITT and H. SCHMIDT, *J. Sol–Gel Sci. Tech.* **8** (1997) 1035.
45. L. C. NISTOR, J. VAN LANDUYT, J. D. BARTON, D. E. HOLE, N. D. SKELLAND and P. D. TOWNSEND, *J. Non-Cryst. Solids* **162** (1993) 217.
46. M. SHEIK-BAHAE, A. A. SAID, T. WEI, D. J. HAGAN and E. W. VAN STRYLAND, *IEEE J. Quantum Electron.* **QE-26** (1990) 760.
47. R. F. HAGLUND Jr, L. YANG, R. H. MAGRUDER III, J. E. WITTING, K. BECKER and R. A. ZUHR, *Opt. Lett.* **18** (1993) 373.
48. P. MAZZOLDI, F. CACCAVALE, E. CATTARUZZA, P. CHAKRABORTY, L. TRAMONTIN, A. BOSCOLO-BOSCOLETTO, R. BERTONCELLO, E. TRIVILLIN, G. BATTAGLIN and G. W. ARNOLD, *Nucl. Instrum. Meth. B* **91** (1994) 505.
49. P. MAZZOLDI, T. TRAMONTIN, A. BOSCOLO-BOSCOLETTO, G. BATTAGLIN and G. W. ARNOLD, *ibid.* **80/81** (1993) 1192.
50. R. H. MAGRUDER III, DO HENDERSON, S. H. MORGAN and A. ZUHR, *J. Non-Cryst. Solids* **152** (1993) 258.
51. H. HOSONO, Y. Y. SUZUKU, Y. ABE, Y. L. LEE, K. OYOSHI and S. TANAKAR, *ibid.* **142** (1992) 287.
52. Y. TAKEDA, T. HOIKI, T. MOTOHIRO and S. NODA, *Nucl. Instrum. Meth. B* **91** (1987) 501.
53. R. H. MAGRUDER III, J. E. WITTING and R. A. ZUHR, *J. Non-Cryst. Solids* **163** (1993) 162.
54. P. D. TOWNSEND, *Rep. Prog. Phys.* **50** (1987) 501.
55. R. C. CARO and R. C. GOWER, *IEEE J. Quantum Electron.* **QE-18** (1982) 1375.
56. W. NIE, *Adv. Mater.* **5** (1993) 520.
57. M. FLEUSTER, CH. BUCHAL, D. FLUCK and P. GUNTER, *Nucl. Instrum. Meth. B* **80/81** (1993) 1150.
58. J. M. ALMEIDA, G. BOYLE, A. P. LEITE, R. M. De LA RUE, C. N. IRONSIDE, F. CACCAVALE, P. CHAKRABORTY and I. MANSOUR, *J. Appl. Phys.* **78** (1995) 2193.
59. F. CACCAVALE, F. SEGATO, I. MANSOUR and P. CHAKRABORTY, in: "Proceedings of the International Conference on Fiber Optics and Photonics", edited by J. P. Raina and P. R. Vaya (Tata McGraw-Hill Publishing Co., New Delhi) India (1996) p. 261.
60. E. DESURVIRE, *Phys. Today* January (1994) p. 20.

Received 1 July 1997
and accepted 27 January 1998